DYNAMIC RESPONSE AND IMPACT DAMAGE DETECTION IN RC BRIDGE PIERS USING FREQUENCY-DOMAIN CORRELATION

SABBANA APPALANAIDU, Assistant Professor, Department of MECH, Avanthi's Research and Technological Academy , Bhogapuram,Vizianagaram,Andhra Pradesh ,India.Email:-appalanaidu.sabbana@gmail.com
OMMI BHAVANI, Assistant Professor, Department of MECH, Avanthi's Research and Technological Academy ,Bhogapuram,Vizianagaram,Andhra Pradesh ,India.Email:-bhavaniommi01@gmail.com
KOMMOJU SRINIVASA RAO, Assistant Professor, Department of MECH, Avanthi's Research and Technological Academy ,Bhogapuram,Vizianagaram,Andhra Pradesh ,India.Email:-kommoju328@gmail.com
POLIPALLI SRINU,Assistant Professor, Department of MECH, Avanthi's Research and Technological Academy ,Bhogapuram,Vizianagaram,Andhra Pradesh ,India.Email:-srinupolipalli31@gmail.com
BUDDA VENKATESH,Assistant Professor, Department of MECH, Avanthi's Research and Technological Academy ,Bhogapuram,Vizianagaram,Andhra Pradesh ,India.Email:-venkatesh.chanti48@gmail.com

ABSTRACT:
We examined the potential applications of damage correlation indices, which are frequency-domain based correlation techniques, to enhance damage detection in reinforced concrete columns. In order to model the impact of medium-sized cars hitting bridge piers, researchers used a new ultra-high drop hammer experiment technique to strike four scaled-down reinforced concrete pier components. The frequency response functions of the members were assessed prior to and following the damage using an acceleration acquisition device. The trials demonstrated that the damage correlation indexes (DCI) that took into account the multi-order modal frequencies were able to effectively assess the damage levels of the piers. Additionally, a modal analysis technique and an impact finite element model were developed and matched with the experiments using the commercial application LS-DYNA. The simulation of the impact processes between medium-sized automobiles and reinforced concrete piers was accomplished by matching the finite element parameters with the experimental data. To make sure that structural design requirements are fulfilled, a peak impact force (PIF) estimate based on damage indices was provided for vehicle crash scenarios.
Key words: Modal frequencies, reinforced concrete piers, lateral impacts, damage identification, and numerical models.

I.INTRODUCTION

The number of vehicles and traffic infrastructure in the area have rapidly increased as a result of the steady acceleration of the urbanization process. As a result, the primary danger to the security of urban overpasses is now car crashes against bridge piers. Many statistical studies on major bridge collapse accidents since the 21st century have been carried out recently; among these, accidents involving ships or vehicles

colliding with bridges have been estimated to account for 20%.1 In these situations, applications of structural health detection technology are especially crucial. Large financial investments are needed for damage assessments and restoration procedures, which could make it impossible to carry out the required activities. Actually, the advancements in computer and sensor technology have led to better options for damage assessment solutions. The most often used data include natural frequencies3, modal shapes4, mass values5, stiffness values6, damping matrixes7, and frequency response functions (FRFs).8 Of the recently introduced technologies, vibration-based monitoring methods allow engineers to gather data in real-time, allowing structures to be evaluated in real-time by comparing the parameters of the original structure with those of the damage state.

Several nations have actively proposed similar design codes to address the impact issues. The most representative code is the planned AASHTO LRFD,9, which bases the design value of bridge piers at 1500 mm from the road edge on the corresponding static force of 2670 KN. Its reasonability was assessed using the original rough finite element model developed by Chen et al.10, and the findings indicated that the values utilized in the aforementioned code were, in certain situations, overly cautious. Therefore, the above-mentioned values were verified using the finite element model presented by Abdelkarim and ElGawady11 and compared with those produced using the equivalent static force calculation method (equation) and a 25 ms average peak force method.

(1)) suggested by Euro-code.12 The findings showed that the comparable static force for structural designs was more logically determined to be the average force of the 25 ms peak force suggested by Buth et al.13:

where m is the vehicle's mass, Vr is its velocity, dc is the variable distance between the vehicle's head and center of mass, and dD is the column's transverse displacement at the impact site. Buth et al.14 conducted transverse impact tests on a full-scale rigid pier model using a 36t tractor-semitrailer. Vehicle head crushing, cargo-pier impact, and other bridge pier mechanical characteristics were all graphically depicted in the model. Chen et al.15 used a medium-sized truck, the Dongfeng-EQ140, to conduct transverse impact tests and built an anti-collision guardrail made up of five short columns. Throughout the experimental procedures, measurements were made of the impact force, deflection, and other variables. A simpler finite element guardrail model was then proposed based on the experimental data that was obtained. Using a transverse impact experimental equipment, Cai et al.16 conducted impact experiments on 15 square scale columns. The aforementioned study focused on how the slenderness ratios affected the impact energy, peak impact force, and member deformations. In a recent work, Zhou et al.17 used an ultra-high drop-hammer experimental setup to investigate the dynamic reactions of concrete pier members under cumulative impact conditions. A damage judgment approach based on changes in modal frequency was devised after the results demonstrated that the internal energy dissipation capacities of the buildings had gradually diminished as the damage degrees increased. Without a doubt, impact experiments that have already been carried out have significantly aided in the advancement of numerical simulations in this area. In order to thoroughly examine the impact mass ratios, longitudinal reinforcement ratios, concrete compressive strength, and other characteristics, Adhikary et al.18 conducted weight reduction experiments on reinforced concrete beams and developed a comprehensive finite element model. Furthermore, Pham and Hao19 developed a simplified mechanical model and a numerical model of reinforced concrete beams, suggested a way to infer shear and

bending moment diagrams, and validated the assumption of linear inertial force distributions along beams because the dynamic behaviors of beams are easier to observe during impact processes. In order to simulate the impact impacts of big vehicles and reinforced concrete columns, Chen et al.20 also created an equivalent impact frame. The equivalency values between the frames and actual trucks were then determined by comparing the deformations and internal energy relations between the two. Lastly, to confirm the general commonalities between them, a suitable finite element simulation was developed. Sharma et al.21 introduced the idea of performance-based design for impact problems and created finite element pier models under various vehicle impact circumstances. Furthermore, a set of program frameworks was developed to estimate the capacities and demands of dynamic shear force in RC columns, and the damages under various states were successfully classified. However, there is no sensible and trustworthy quantitative index, and the performance design criteria used to classify bridge pier safety grades are too ambiguous. A high-applicability calculating approach for impact forces and damage evaluation indices was suggested in the study. The studies in this paper used trucks to perform simplified impact tests on circular section piers on a smaller scale. Measurements were made of the RC columns' dynamic reactions during impact and the modal frequency variations following member destruction. A comprehensive finite element model was then developed in accordance with the experimental findings, and the experimental results were confirmed using LS-DYNA software22. Additionally, a full-scale pier under impact conditions was modeled using finite elements. The numerical simulations conducted for this study showed the connections between the peak impact

$$ESF = \frac{mv_r^2}{2(\delta_C + \delta_D)} \quad (1)$$

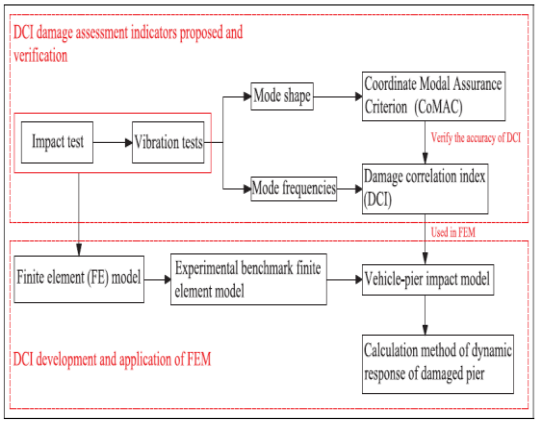

Figure 1. The tests' technical route diagram.

force (PIF) and the levels of damage. Then, taking into account the age of the bridge pier, an equivalent static force calculation formula for vehicle hits in a brief amount of time was developed. This formula may potentially offer useful references for structural designs in the future. Figure 1 displays the research techniques used in this article.

Techniques for evaluating damage based on frequency domains

The dynamic response shift brought on by damage is the foundation of the vibration-based impact damage assessment approach. This phenomenon enables the identification of damage resulting from a change in dynamic responsiveness. Two categories of damage indicators are presented in this section. Modal Assurance Criterion (MAC)23 and Coordinate Modal Assurance Criterion (CoMAC)24 are two indicators that are used to represent how the mode shape differed before and after the reinforced concrete structure was damaged. The distinction is that COMAC takes into account the deviation of the multi-order mode shape, whereas MAC simply takes into account the deviation of the first-order mode shape. The damage correlation coefficient (DCI), which can show the variation in multi-mode frequencies

prior to and following structural damage, is the second. The proposed damage index DCI for impact damage is the subject of verification in this study, while CoMAC is regarded as a conventional damage assessment index.

2. MAC and CoMAC

Equation (2) illustrates that the MAC, a dimensionless scalar constant, is a measure of the degree of correlation between the modal vector and another reference modal vector. The co-ordinate modal assurance criterion (COMAC)24 is an extension of the modal assurance criterion (MAC), and its correlation is modal related. In the equation, CAi stands for the i-order modal vector from State A. Equation (3) indicates that the j-order mode form at location i in State A is CAij:

$$\mathrm{MAC}(\{\psi_{\mathrm{A}i}\},\{\psi_{\mathrm{B}j}\}) = \frac{\left|\{\psi_{\mathrm{A}i}\}\{\psi_{\mathrm{B}j}\}\right|^2}{(\{\psi_{\mathrm{A}i}\}^t\{\psi_{\mathrm{A}i}\})(\{\psi_{\mathrm{B}j}\}^t\{\psi_{\mathrm{B}j}\})} \quad (2)$$

$$\mathrm{COMAC}(\{\psi_{\mathrm{A}ij}\},\{\psi_{\mathrm{B}ij}\}) = \frac{\sum_{j=1}^{N}\left|\{\psi_{\mathrm{A}ij}\}\{\psi_{\mathrm{B}ij}\}\right|^2}{\sum_{j=1}^{N}\{\psi_{\mathrm{A}ij}\}^2\sum_{j=1}^{N}\{\psi_{\mathrm{B}ij}\}^2} \quad (3)$$

Damage correlation index (DCI)

Index of damage correlation (DCI)

The original modal frequency and the damage modal frequency were compared and contrasted in order to assess the damage levels in this investigation. The differences between the two samples were assessed using the quantitative value. The problem could be solved using the sample Pearson Correlation Coefficient (PCC)25 as a correlation. The two states of health and damaged are denoted by A and B, respectively, in equation (4). In the structural health condition, Ai stands for the i-th order modal frequency. SA is the standard deviation of the frequency sample in the healthy state, and A is the mean value of the frequency sample in the healthy state:

$$\mathrm{PCC}_{\mathrm{A,B}} = \frac{\sum_{i=1}^{n}(\mathrm{A}_i-\overline{\mathrm{A}})(\mathrm{B}_i-\overline{\mathrm{B}})}{(n-1)\sigma_{\mathrm{A}}\sigma_{\mathrm{B}}} \quad (4)$$

$$\overline{\mathrm{A}} = \frac{1}{n}\sum_{i=1}^{n}\mathrm{A}_i \quad (5)$$

$$\sigma_{\mathrm{A}} = \sqrt{\frac{1}{n-1}\sum_{i=1}^{n}(\mathrm{A}_i-\overline{\mathrm{A}})^2} \quad (6)$$

For real numbers with a PCC value of [21,1], the reverse or indirect correlation between the data sets under comparison is represented by 21, the linear correlation by 1, and the complete correlation by 0. However, since they represent the opposite correlation of the frequency, such occurrences are not included in our analysis. Thus, the damage correlation coefficient (DCI) could be computed if PCC is bounded within the interval [0, 1]. Determining that the DCI value was 0 when the column was intact and 1 after the correlation was totally gone was simple:

$$\mathrm{DCI} = 1 - |\mathrm{PCC}_{\mathrm{A,B}}| \in R \quad (7)$$

Experimental processes and analysis results

Procedures used in experiments and analytical findings

The purpose of this study is to examine the effects of the effective loss characteristic index. It was conducted in two stages: first, using a lateral member percussion impact system, and subsequently, using modal parameters evaluated by a vibration test following injury. Four circular cross-section bridge pier components with a 1:3 scale are constructed for this investigation. The test model is scaled according to Buckingham's p theory, and the precise dimensions of the bridge pier model are provided in Section "Vehicle-bridge impact

model." Make that the materials used for the full-scale bridge piers and the scaled components are the same during the pouring operation. Currently, the material attributes have a 1:1 scale effect:

3. EXPERIMENTAL PROCESSES

getting the damaged parts ready. Figure 2 displays the detailed specimens. A circular RC column with a section radius of 170 mm and a height of 2200 mm made up each specimen, which also included a 900 3 300 3 400 mm3 RC base. Concrete having a cube compressive strength of 42 MPa was used to cast each specimen.

A vertical drop-hammer driving system and a horizontal impact system made up the super-high heavy-duty drop-hammer experimental testing machine system used for the impact test (Figure 3). The vertical drop-hammer driving system supplied the horizontal impact test vehicle's kinetic energy, as seen in Figure 3(a). Equation (8) illustrates the conversion connection, where m1 and m2 stand for the steel impactor mass and the drop weight mass, respectively, and g is the

acceleration of gravity, m is the track dynamic friction coefficient, and h is the drop weight's release height. The fundamental details of the experimental elements and the affecting methodology are provided in Table 1. The cumulative impact shows how the degree of damage affects the column's dynamic response:

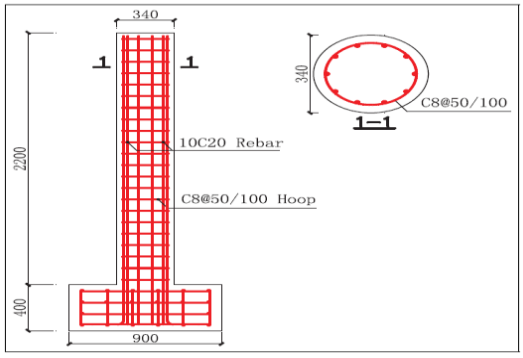

Figure 2. Specimen dimensions and detailed.

acceleration of gravity, h represents the release height of the drop weight, and m is the track dynamic friction coefficient. Table 1 details the basic information of the experimental components and the impacting scheme. The impact of the damage degree on the dynamic response of the column is reflected by the cumulative impact:

$$0.5 \times (m_1 + m_2)v_0^2 + \mu m_1 g = m_2 g h \qquad (8)$$

Vibration tests. This study's modal tests were carried out on the damaged components after impact. Uninstall axial load in order to ensure the axial force is not involved in the test, and the upper portion of the col- umn is maintained free vibration. Vibration testing system shown in Figure 4(a) and (b), 10 accelerometers were distributed in the direction of impact specimen back (Figure 4) to ensure that the measured third-order modes. Externally stimulated the front of the impact until the column frequency measurement results are stable. Wherein the accelerometers was used to measure the vibration characteristics of the pier during excita- tion, then the data transmitted to the data logger, the last time domain signal was collected by the computer and obtain a frequency domain data by Fast Fourier Transform. Figure 4(c) shows the acceleration time-domain data collected by the damaged column C1. It is not difficult to observe that the frequency of each order of the damaged column decreases, especially at the higher order frequencies. The appropriate number of accelerometers to ensure the accuracy of the experiment.

Table 1. Information of the components

Specimen	Longitudinal reinforcement ratio ρ_0 (%)	Hoop reinforcement ratio ρ_v (%)	Impact velocity at first-second-, third loading (V_1–V_2–V_3) (m/s)	Axial compression ratio ρ_n (%)
C1	10C20 (2.7)	8@50 (1.7)	4.5	30
C2			4.5–4.5–4.5	20
C3		8@100 (0.9)	4.5–4.5	20
C4		8@150 (0.5)	4.5	20

The axial compression ratio is calculated by $\rho_n = F_{axial}/(\pi r^2 f_c + A_s f_y)$.

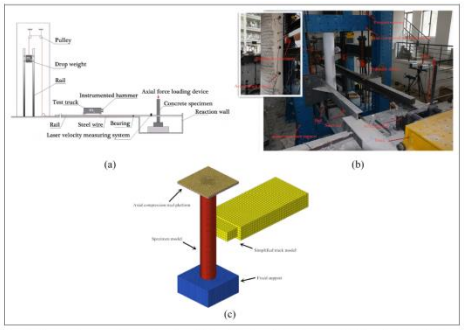

Figure 3. Impact testing system: (a) experimental test 2D view, (b) horizontal impact system, and (c) FE model of the RC column with the steel impactor.

Stiffness measurements. It is necessary to measure the change in the overall stiffness of the column, but the shear stiffness and bending stiffness cannot be made in detail to distinguish during the experiment, the stiffness variation will be described using the overall stiffness of the column in this study. Following impact, the axial pressure was unloaded in order to ensure that the upper rigid plate was no longer in contact with the column. Equal increment transverse force (100 kn, 200 kn, and 300 kn) was applied to the top of the column using the reaction wall. The magnitude of the force was recorded by a dynamometer, and the displacement changes were recorded using a displacement meter installed on the top of the column, as shown in Figure 5, in which Dd represents the displacement differences. Equation (9) was used as the calculation formula of the column stiff- ness, E is the modulus of elasticity, and I is the moment of inertia of the section.

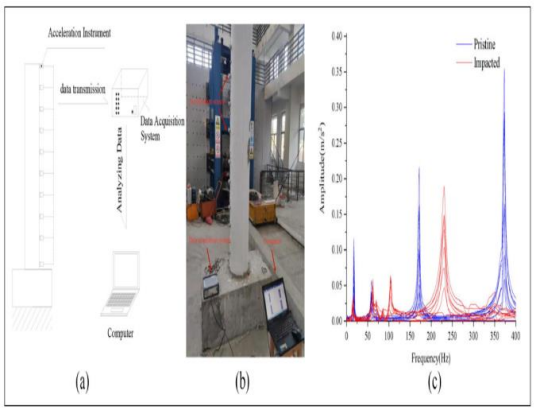

Figure 4. Modal testing system: (a) analytic flowcharts, (b) experimental facility, and (c) comparison of frequency response plots of post-impact and original RC piers.

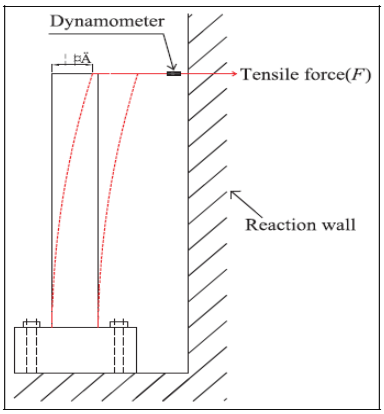

Figure 5. Stiffness measurement system.

$$K = \frac{3EI}{l^3} = \Delta F / \Delta \delta \qquad (9)$$

4. EXPERIMENTAL RESULTS AND ANALYSIS

modal tests. The comparison of the findings of the experimental identifications of the natural frequencies in this study is shown in detail in Figure 6 and Table 2. It was discovered that the parts where cracking happened had less stiffness as a result of the cumulative blows. When the damage was minor, the change of the first-order frequency was not sensitive, and the extent of damage could not be described.26 The decreases in natural frequencies brought on by the formation of fractures were not monotonic. The results of the DCI computation demonstrated that because multi-order modal frequencies were taken into account, this index was very susceptible to damage. In contrast to the CoMAC development trend, the DCI will rise as the extent of injury grows. Using DCI as an evaluation indication makes more sense than relying solely on the first-order modal frequency.

Likewise, it was impossible to overlook the modal shape modifications. Component C2's modal shape measurement findings before and after impact are displayed in Table 3. Changes in damage degrees had no effect on the geometry of the first-order mode. However, it was possible to make a preliminary determination about the

damage locations by looking at the change processes of the second- and third-order mode forms. The method's efficiency is demonstrated by the density of the cracks at this area.

impact tests. The correlations between the damage levels of component C2's three impact forces and changes in time history are displayed in Figure 7. The column DCI rises and the peak impact force (PIF) falls with increasing column damage. It was discovered that the peak impact force was not significantly impacted by the lesser losses in the stiffness values. After two collisions, however, the pier responses were notably diminished. The responses were weakened as a result of the column's lack of rigidity.

Verification of stiffness. The procedure outlined in Section "Stiffness measurement" was used to determine the changes in the stiffness values of the components before and after impact. Table 4 provides statistics on the rates at which the stiffness values of each component changed.

A number of natural frequencies changed as a result of the impacts' reductions in the total structural stiffness. The evolution of this issue

Figure 6. The components' modal frequencies are (a) undamaged modal frequencies and (b) damaged modal frequencies.

Table 2. Results of modal tests

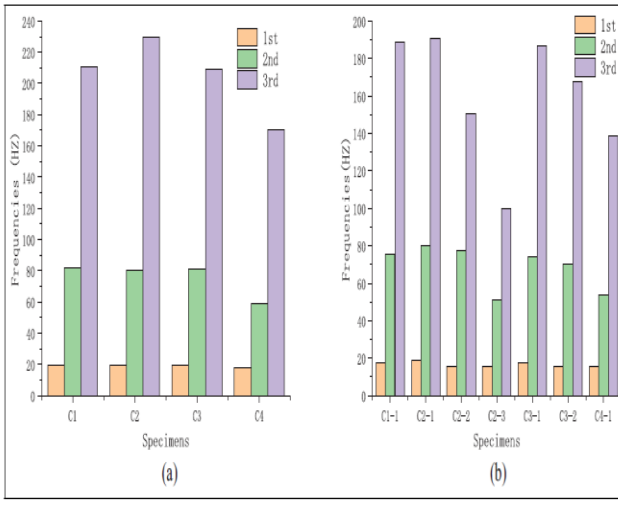

Figure 6. Modal frequencies of the components: (a) modal frequencies (undamaged) and (b) modal frequencies (damaged).

Table 2. Modal test results

Specimens	Experimental			FEM			CoMAC	DCI
	Frequencies	DIFF (%)	Stiffness change (%)	FEM-PRED	Frequencies	DIFF (%)		
C1								
Undamaged			0	0		2.82	1	0
1st-order	19.53				18.98	10.29		
2nd-order	82.03				90.46	2.63		
3rd-order	210.99				205.44			
Impact-1			50.62	0.16		2.54	0.971	0.0001
1	17.57	−9.99			17.13	2.90		
2	75.70	−7.71			73.51	4.24		
3	188.95	−10.44			180.94			
C2								
Undamaged			0	0		2.82	1	0
1	19.53				18.98	12.74		
2	80.24				90.46	10.48		
3	229.49				205.44			
Impact-1			49.77	0.18		10.22	0.984	0.00255
1	19.08	−2.29			17.13	7.87		
2	79.79	−0.56			73.51	5.13		
3	190.73	−16.89			180.94			
Impact-2			68.29	0.23		2.68	0.966	0.01037
1	15.74	−19.36			15.32	2.80		
2	77.71	−3.15			75.53	6.66		
3	150.36	−34.48			140.35			
Impact-3			79.43	0.47		14.68	0.931	0.01858
1	15.74	−19.36			13.43	0.31		
2	50.78	−36.72			50.93	5.86		
3	99.60	−56.60			93.76			
C3								
Undamaged				0		1.21	1	0
1	19.21				18.98	2.80		
2	81.21				83.48	6.74		
3	208.73				194.67			
Impact-1			36.04	0.12		2.10	0.977	0.00005
1	17.58	−8.46			17.21	0.96		
2	74.30	−8.50			73.59	4.64		
3	186.31	−10.72			177.67			
Impact-2			46.92	0.33		3.80	0.963	0.00068
1	15.62	−18.67			15.03	2.25		
2	70.31	−13.42			71.89	2.61		
3	167.47	−19.76			171.85			

Table 2. (Continued)

Specimens	Experimental			FEM			CoMAC	DCI
	Frequencies	DIFF (%)	Stiffness change (%)	FEM-PRED	Frequencies	DIFF (%)		
C4								
Undamaged				0		2.29	1	0
1	17.57				17.98	30.51		
2	58.59				76.47	10.32		
3	169.99				187.53			
Impact-1			78.48	0.19		9.66	0.971	0.00094
1	15.48	−11.91			13.98	14.73		
	53.54	−8.61			61.43	10.85		
3	138.67	−18.42			153.71	2.82		

The DIFF: under the Experimental describes the initial frequency of the column and the frequency change after column damage; the DIFF: in the FEM describes the difference between the finite element calculation results and the experimental results.

Table 3. Comparison of the modal shapes of component C2.

Specimens	Mode shapes-undamaged	Mode shapes-damaged
C2-1	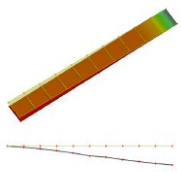	1st 2nd 3rd
C2-2	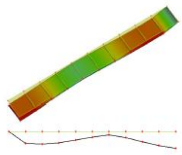	1st 2nd 3rd
C2-3	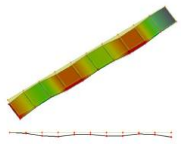	1st 2nd 3rd

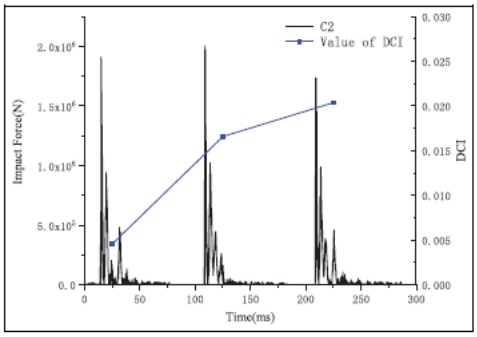

Figure 7. Comparison of the impact force time history and DCI changes of Component C2.

Table 4. Changes in the stiffness.

Specimen	Stiffness *K* (kn/m)	Change ratio (%)
C1		
Undamaged	8052.3	
C1-1	3976.4	50.62
C2		
Undamaged	7436.2	
C2-1	3734.8	49.77
C2-2	2357.7	68.29
C2-3	1529.6	79.43
C3		
Undamaged	6555.8	
C3-1	4192.8	36.04
C3-2	3479.6	46.92
C4		
Undamaged	6713.3	
C4-1	1444.6	78.48

mostly arose from the system vibration equation's characteristic value issue. Thus, the undamped mechanical system's motion equation (10) was used. The Rayleigh Method27 was used to solve the experimental model's first third order frequency approximation, and the accuracy of the experimental data was effectively confirmed. Equation (11) was thus developed in accordance with the energy conservation principle, which states that the strain energy at the maximum displacement time is equal to the beginning kinetic energy.

When considering only one direction of displacement, the strain energy expression of a cantilever beam looks like this:

$$\frac{\partial^2}{\partial x^2}\left[EI(x)\frac{\partial^2 v(x,t)}{\partial x^2}\right] + m(x)\frac{\partial^2 v(x,t)}{\partial t^2} = p(x,t) \quad (10)$$

$$U_{max} = W_{max} \quad (11)$$

The strain energy expression of a cantilever beam con- sidering only the displacement in one direction is as follows:

$$W_{max} = \frac{1}{2}\int_0^l EI\left(\frac{\partial^2 y}{\partial x^2}\right)^2 dx \quad (12)$$

The kinetic energy expression is as follows:

$$U_{max} = \frac{1}{2}\omega^2 \int_0^l my^2(x)dx \quad (13)$$

Therefore, according to equations (10)–(13), the follow- ing was obtained:

$$\omega^2 = \frac{\int_0^l EI\left(\frac{\partial^2 y}{\partial x^2}\right)^2 dx}{\int_0^l my^2(x)dx} \quad (14)$$

In the current study, based on the above-mentioned method, the natural vibration frequencies of the cantile- ver components under the effects of gravity were solved and the first three order approximate solutions were determined as follows:

$$\omega_1 = \frac{3.5160}{l^2}\sqrt{\frac{EI}{m}}\omega_2 = \frac{22.0345}{l^2}\sqrt{\frac{EI}{m}}\omega_1 = \frac{61.6972}{l^2}\sqrt{\frac{EI}{m}} \quad (15)$$

The expressions of the structural stiffness were deter- mined (equation (16)), and the structural stiffness were C3 obtained using the calculations detailed in Table 4:

$$K = \frac{3EI}{l^3} \Rightarrow EI = \frac{Kl^3}{3} \quad (16)$$

In the present research investigation, by comparing the experimental results with the theoretical calculation results, the accuracy levels of the experiments were veri- fied. It was not difficult to determine through the find- ings of the experiments that the low-order frequencies were insensitive to the stiffness degradation phenom- enon. This had led to deviations in the measured values from the theoretical approximate solutions. Since this study's experimental processes could not ensure stable fixed boundaries, elastic treatments of the boundaries will be required in order to achieve more accurate calcu- lations. However, the experimental results showed that there were reasonable correlations between the DCI and stiffness changes (Figure 8). Therefore, it was con- sidered that in engineering practices, the measured com- ponent frequency changes could be used to accurately predict the degrees of stiffness loss.

Table 5. Comparison of the theoretical calculations and the experimental data.

Specimens	Frequencies (HZ)								
	1st			2rd			3nd		
	Theo	Exp	Error (%)	Theo	Exp	Error (%)	Theo	Exp	Error (%)
C1	13.30	19.531	31.903	83.38	82.031	−1.645	233.46	210.993	−10.648
C1-1	9.35	17.578	46.809	58.59	75.703	22.605	164.06	188.953	13.174
C2	12.79	19.531	34.514	80.12	80.242	0.152	224.35	229.492	2.241
C2-1	9.06	19.083	52.523	56.78	79.791	28.839	159.00	190.736	16.639
C2-2	7.20	15.749	54.283	45.12	77.717	41.943	126.33	150.365	15.984
C2-3	5.80	15.749	63.172	36.34	50.781	28.438	101.75	99.609	−2.149
C3	12.00	19.213	37.542	75.23	81.212	7.366	210.65	208.73	−0.920
C3-1	9.60	17.588	45.417	60.16	74.304	19.035	168.47	186.314	9.577
C3-2	8.75	15.625	44.000	54.81	70.313	22.049	153.47	167.476	8.363
C4	12.15	17.578	30.880	76.13	58.594	−29.928	213.17	169.992	−25.400
C4-1	5.64	15.484	63.575	35.32	53.547	34.039	98.89	138.672	28.688

In the table, C2-1 represents the experimental data of the C2 member following the first impact; Test represents the experimental result.

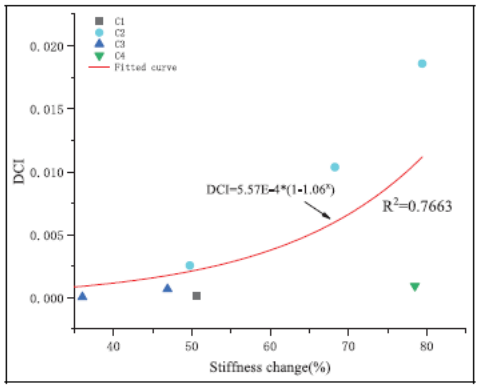

Figure 8. Correlations between the DCI and stiffness losses.

Numerical simulation and discussion

A finite element model which matched with the experi- ments was established using LS-DYNA commercial software. After analysis of the collision by explicit anal- ysis, modal analysis by its implicit analysis. This section calibrates the finite element model and describes the solution to the conversion between algorithms.

Finite element (FE) model

The adopted 3D nonlinear finite element analysis model based on the experimental model is shown in Figure 3(c). Both the concrete and steel impacting cars adopted hexahedral elements with single integral points, and the reinforcement elements adopted Hughes-Liu sectional integral beams of 2 3 2 Gauss integral elements. Also, both the longitudinal reinforcements and the stirrups were regarded as elastic-plastic materials, which could be reasonably described using a piecewise nonlinear model. In this study, the dynamic intensification factor (DIF) rela- tionships provided by Li and Hao28 were used to consider the strain rate effects. The relationships between the strain rates and DIF were obtained using equation

(17). The model was described using multi-stage elastic- plastic curves. In the current investigation, DIF = 1 represented the material state description under the quasi-static conditions. The corresponding yield point could then be expressed as the material changes from an elastic state to a plastic state when the stress level reached 350 MP and the strain reached 0.2%. As shown in Figure 3(b), the superstructure in the experi- ments was an axial hydraulic loading platform, and the keyword named *LOAD_BODY_Z was used in the numerical model in order to apply the gravity load to the entire model, and was equivalently simplified with an elastic material of suitable mass. The mass of the elastic material could be adjusted by changing its thick- ness. Similarly, due to the fact that the stiffness of the RC structure was far less than that of the steel trolley, the steel trolley was simplified as an elastic material for calculation purposes. Table 6 details the material parameters:

$$\mathrm{DIF}_s = \left(\frac{\dot{\varepsilon}}{10^{-4}}\right)^{0.074-0.040\frac{f_y}{414}} \qquad (17)$$

In the current study, LS-DYNA contact keyword *CONTACT_SURFACE TO SURFACE contact algo- rithm was used between the mass object and column, and the keyword named *CONTROL_DYNAMIC_ RELAXATION was used for the dynamic relaxation analysis of the structure 0.1 s prior to the calculation in

Table 6. Model material parameters.

Type	Material modal	Parameter	Magnitude
Longitudinal rebar	PIECEWISE_LINEAR_PLASTICITY (*MAT_024)	Mass density	7850 kg/m^3
		Modulus of elasticity	205,000 Mpa
		Poisson's ratio	0.3
		Yield stress	400 MPa
		Failure strain	0.4
Stirrup	PIECEWISE_LINEAR_PLASTICITY (*MAT_024)	Density	7850 kg/m^3
		Modulus of elasticity	205,000 Mpa
		Poisson's ratio	0.3
		Yield stress	335 MPa
		Failure strain	0.4
Steel plates, Steel impactor	ELASTIC (*MAT_03)	Mass density	7850 kg/m^3
		Modulus of elasticity	205,000 Mpa
		Poisson's ratio	0.3
Concrete	CSC Modal (*MAT_159)[22]	Mass density	2490 kg/m^3
		Compressive strength	42 MPa
		Maximum aggregate size	15 mm
		EROD	1.1
		RECOV	10.4

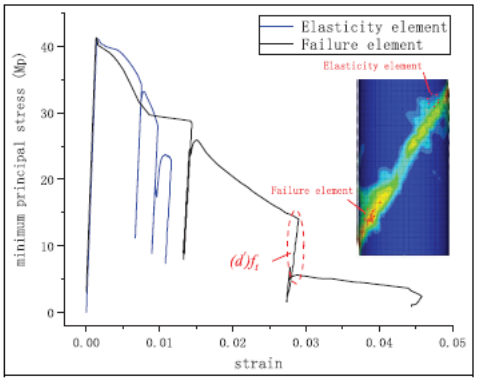

Figure 9. Cylinder model and result diagram.

in order to guarantee the axial force application's stability. The concrete grid size was then set at 10 mm in accordance with Yuan et al.29's research findings on grid size sensitivity. Furthermore, the steel impact trolley might be considered a rigid body because of the little deformations that occurred throughout the contact procedures. Its grid was therefore split into 50 mm sections. CONSTRAIN_BEAM IN SOLID was used to take into account the slip effects between the reinforced concrete and the reinforcement in relation to the contact setting.

Validation of concrete material models

The main evidence for the validity of the CSC modality is that the plastic deformation is assessed for reasonableness and the unloading stress is found to be reasonable. Figure 9 illustrates the basic finite element model of the F150*300 mm cylinder that was put up by Malvar,30. A displacement technique was used to model the cylinders' axial compression trials and perform cyclic loads. In a previous section, the material parameter settings were explained. When compared to experimental and finite element model results in the literature, the model was able to accurately reflect the effects of stiffness degradation during the damage accumulation processes. Figure 9 illustrates the stress-strain development process of the elastic element and the failure element during the loading process. In a similar manner, the established experimental model was used to perform trial calculations of the concrete constitutive model. The impact force time history and crack development of Component C4 as observed in the experiment are displayed in Figure 10, and the outcomes of the numerical calculations and the experimental data were contrasted. The findings demonstrated that the constitutive model could accurately forecast both the impact force's peak magnitude and its evolution in low velocity impact scenarios. It was found that there were less than 10% variations between the calculated and experimental findings.

Modal analysis of the model that is damaged

The numerical calculations needed to account for pre-existing damages because of the oblique punching cracks (Figure 10) that developed after impact. This problem was logically resolved by the pre-existing damage (PRED) characteristics that the CSC model offered. The modal analysis was

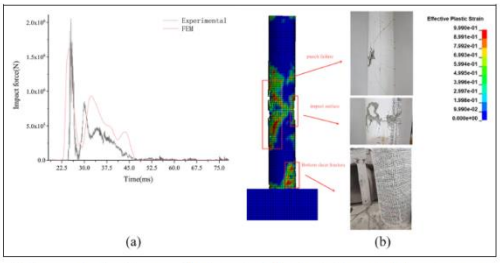

Figure 10. Experimental results of Component C4 and comparison of the value calculation results: (a) dynamic responses of specimens C4 and (b) impact damage of specimens C4.

Table 7. Comparison of the modal frequencies under different damage degrees.

Model frequencies/ PRED	0	0.1	0.3	0.5	0.7
1st	22.3851	21.57	19.67	17.50	15.57
2nd	98.4437	94.48	85.58	75.70	63.98
3nd	230.4552	217.99	192.20	162.93	126.98

carried out for the same calculation model under conducted using different PRED values for the same computation model; the outcomes are displayed in Table 7. It was discovered that the modal frequencies decreased nonlinearly as the PRED values increased.

Studying the cumulative damage issues of RC piers and modal analysis is made possible by restart technology. These issues were investigated through experiments and numerical simulations by Kishi et al.33. The KISHI approach, however, was limited to situations involving collisions between simple rigid bodies; it was not suitable for nonlinear big deformation impact problems involving complex structures and numerous failure causes. As a result, this study offered the following novel restart technique: 1. After the first computation, the experimental data was compared and the calculation results were verified using the post-processing program Ls-Prepost. When the computation results were determined to be accurate, the element and nodes were exported using Ls-Prepost's exported option so that they could be employed in a geometric model for the subsequent computation.

2. In order to create a stress-strain initialization file at the start of the second calculation, the initial damages were applied to the material at the same time that the stress and plastic strain of every element at the conclusion of the first calculation were output using the DYNAIN option in Ls-Prepost.

3. The second impact file was then obtained by resetting the solution choices, assembling a geometry file, and creating a stress initialization file. It was important to note that the model could be suitably simplified by deleting the upper steel plate and the steel trolley, as well as by switching the solver to implicit analysis, when the modal analysis files were being assembled.

To guarantee the precision of the modal computations in the present study, the PRED values were modified to guarantee that the MAC values

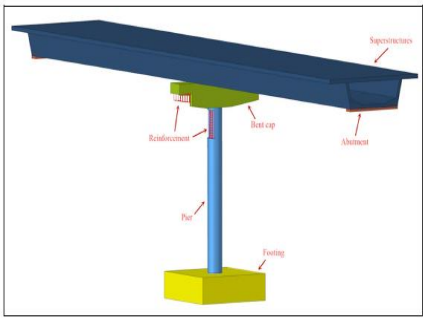

Figure 11. Specific sizes of the pier models.

were in the acceptable range. The range was then separated to make the computation procedure easier. The numerically determined modal frequency values are displayed in Table 7. The findings demonstrate that the computation approach is appropriate for the current investigation.

Impact model between vehicles and bridges

Additionally, the DCI can offer engineering design references. Numerous numerical simulation calculations were performed using columns with varying section sizes, impact velocities, and vehicle masses in order to examine the relationships between the modal frequencies and dynamic responses of bridge piers under the effects of cumulative impacts of vehicles. The findings demonstrated that the cargo mass and velocity values controlled two different kinds of impact forces at the moment of impact. It was discovered that the proper finite element analysis parameters may be identified based on the experimental results. The validity of the DCI damage indicators utilized in this study was then confirmed by combining them with a full-scale model of the pier and the

Ford F800 medium truck model created by the National Crash Analysis Center (NACA). The relationship between damage degree and dynamic responsiveness was examined using regression analysis.

Details on the trucks and piers

This study used the same modeling approach as outlined in Section "Concrete material model validation," which included the material model, contact mode, and strain rate effect factors, to guarantee the validity of the finite element model. The prototype problem, which consists of a circular single column, superstructure, and two supports, was simplified by Consolazio et al., who suggested that a bridge model made up of bridge columns and two spans can accurately anticipate the dynamic response of a multi-span bridge. In order to transfer the weight of the superstructure with a length of 30 meters to the pier column, a trapezoidal solid beam was placed on top of the concrete foundation, which had dimensions of 5000 mm by 5000 mm by 1200 mm, as illustrated in Figure 11. In order to maintain the same axial compression ratio in all crash scenarios, its weight varied according to the size of the column section. Table 8 displays every instance of a collision. Rubber bearings held the column and the bridge pier's superstructure together. According to earlier studies by EI-TAWIL et al., the pier's total dynamic response is barely impacted by the stiffness of the support. Using the LS-DYNA keyword CONTACT AUTOMATIC SURFACE TO SURFACE, it is anticipated that the vertical component of the pier will make contact with the concrete surface.

The Ford vehicle model was utilized to depict the collision of the car on the bridge pier, as seen in Figure 12. Abdelkarim et al.11 and Sharma et al.21 shared the model and conducted experimental testing to confirm its accuracy. The Ford truck's overall mass in this study's model was 8 t, which included 2.8 t of payload and 0.24 t of engine mass. Elastic materials with elastic moduli of 11,000 MP and 2000 MP were used to mimic the engine and cargo. By altering the commodities' quality, the vehicle model's weight was managed.

Impact responses of vehicles

PIF stands for peak impact force. The cumulative impact reflects the shift in the degree of damage. The usual time

Table 8. Numerical simulations of the component information.

scenarios	Column size (mm)	Longitudinal reinforcement ratio ρ_0 (%)	Hoop reinforcement ratio ρ_v (%)	Axial compression ratio ρ_n (%)
C800-V60-W8 C800-V90-W8 C800-V110-W8	800	10C22 (0.756)	25@150 mm (1.31)	388 t (40.5)
C1000-V60-W8 C1000-V90-W8 C1000-V110-W8	1000	10C28 (0.784)	25@150 mm (1.08)	612.95 t (40.5)
C1200-V60-W8 C1200-V90-W8 C1200-V110-W8 C1200-V60-W10 C1200-V90-W10 C1200-V110-W10 C1200-V60-W12 C1200-V90-W12 C1200-V110-W12	1200	10C32 (0.711)	25@150 mm (0.95)	859.6 t (40.5)

In the table, C800-V60-W8-1 indicates that the 800 mm diameter column is the first to be impacted by the vehicles with a total weight of 8 t and a speed of 60 km/h; 10C22 means 10 steel bars with a diameter of 22 mm; 25@150 means that the stirrup spacing is 150 mm and the diameter is 25 mm.

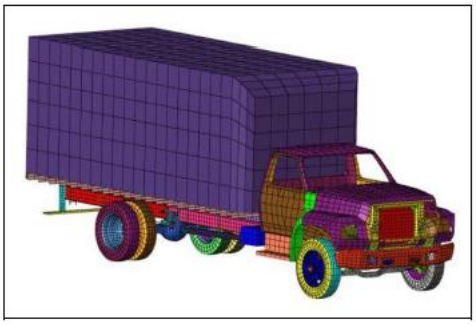

Figure 12. Truck model.

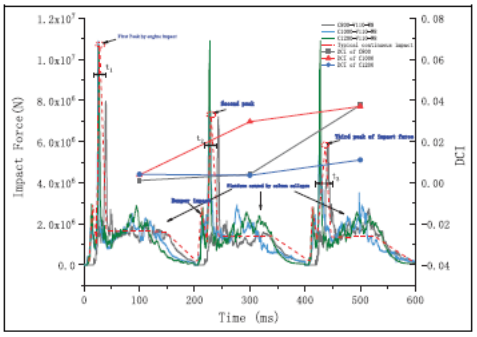

Figure 13. Time history diagram of the typical continuous impact force and damage degrees of the bridge piers.

Figure 13 displays the timeline of the three successive impacts together with the corresponding DCI values. A time history diagram of the V110-W8 component's three impact forces (C800, 1000, and 1200) is shown in the figure. The second impact's end time and the third impact's start time were 400 ms and

200 ms, respectively, for each calculation time. The engine's collision with the bridge pier was the source of all three impact forces' peak values. Thus, based on the comparison results, the first typical impact force's time history diagram matched the shape of the impact force's time history diagram created by Chen et al.34 and Cao et al.35. Figure 14 uses the effective plastic strain following impact to describe the component damage levels. The components' modal parameters eventually deviated from their initial states as a result of the accumulation of impact times, and the PIF values decreased as a result of the stiffness values decreasing. It was discovered that this condition was typical of piers that had experienced mishaps. It was also important to note that in C1200-V110-W8, this behavior was not readily apparent. This was because it was difficult for the medium-sized truck's impacting forces to alter the stiffness values of the pier of that specific size at that speed. The results indicate that DCI values rise as the degree of damage rises, as seen in Figures 13 and 14. Demonstrate the efficacy of DCI pier damage detection for a more robust resistance to piers, which increase in value more slowly.

Peak values, length Tn, and 25 ms are among the statistical information of the numerical simulation results of the columns with varying sizes that are detailed in Table 9.

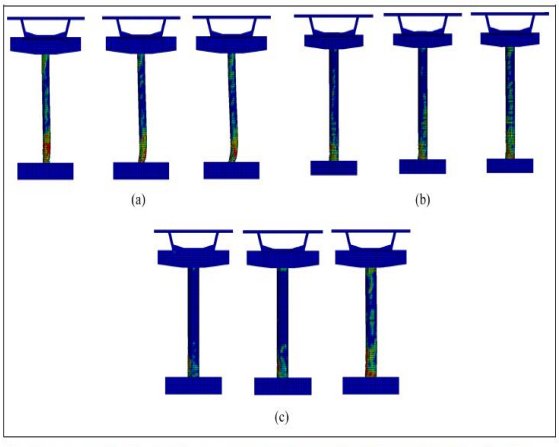

Figure 14. Comparison of the impact damage degrees: (a) C800-V110-W8, (b) C1000-V110-W8, and (c) C1200-V110-W8.

Table 9. Numerical simulation results.

Scenarios	First impact			Second impact			Third impact		
	PIF (MN)	ESF (MN)	DCI	PIF	ESF	DCI	PIF	ESF	DCI
C800-V60-W8	2.27	1.510	0.00033	2.52	1.546	0.00546	2.4	1.537	0.00736
C800-V90-W8	7.08	2.069	0.00060	6.35	2.131	0.01363	7.16	2.092	0.02769
C800-V110-W8	9.88	2.175	0.00105	7.86	2.526	0.01641	5.85	2.752	0.03779
C1000-V60-W8	2.12	1.450	0.00028	2.22	1.494	0.00058	2.13	1.530	0.00104
C1000-V90-W8	8.2	2.314	0.00069	6.73	2.337	0.00186	7.06	2.225	0.01035
C1000-V110-W8	10.9	2.423	0.00379	7.85	2.852	0.02971	6.38	2.714	0.03709
C1200-V60-W8	3.01	1.621	0.00019	3.23	1.634	0.01150	2.75	1.507	0.02445
C1200-V90-W8	8.89	2.224	0.00054	8.16	2.106	0.00103	6.4	2.178	0.00901
C1200-V110-W8	10.7	2.549	0.00411	10.7	2.532	0.00355	7.93	2.533	0.01107
C1200-V60-W10	3.07	1.601	0.00004	2.62	1.537	0.00121	2.70	1.554	0.00335
C1200-V90-W10	8.01	2.374	0.00025	6.08	2.350	0.00177	7.85	2.428	0.01308
C1200-V110-W10	11.9	2.523	0.00749	8.89	2.687	0.014437	8.39	2.428	0.02547
C1200-V60-W12	3.14	1.595	0.00029	2.57	1.549	0.002741	2.95	1.563	0.01451
C1200-V90-W12	8.14	2.253	0.00643	7.34	2.297	0.017594	4.37	2.181	0.02314
C1200-V110-W12	12.20	2.553	0.00314	6.39	2.731	0.019881	6.32	2.662	0.02495

comparable static computation outcomes for every impact force. A medium-sized vehicle weighing 8 t had an impact on every component in the chart, representing a common engine impact situation.

EI-TAWIL's research [40] demonstrated that the American Association of State Highway and Transportation Officials' (AASHTO) peak force calculation (equation (18)) for ship-bridge collisions also applied to vehicle impacts. The formula took into account the hitting bodies' mass W (kg) and impact velocity V (m/s). A new expression equation (20) for the pre-damaged impact problem was proposed in this study, along with two dimensionless parameters: the damage factor DCI and the

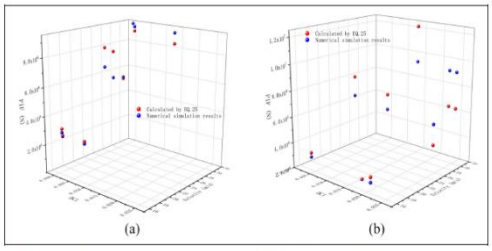

Figure 15. Comparison between simulation results and equation (20): (a) C1200-W10 and (b) C1200-W12.

They introduced equal stiffness (b/800). As a result, the formula succeeded in providing a more thorough explanation of every parameter. Using a nonlinear regression analysis method, five regression coefficients (abbreviated a, b, c, d, and e) were found. It was discovered that equation (20) might be used to estimate the PIF engine when it was continuously impacted. The fitting results and the numerical simulation results from this investigation are compared in detail in Figure 15.

$$F_i = f\{\alpha(V)^{\beta}(W)^{\gamma}\} \quad (18)$$

$$PIF = f\left\{a(DCI)^{b}(V)^{c}(W)^{d}\left(\frac{b}{800}\right)^{e}\right\} \quad (19)$$

$$PIF_{engine} = 10027.08(DCI)^{-0.044}(V)^{2.13}(W)^{-0.085}\left(\frac{b}{800}\right)^{0.364} \quad (20)$$

5. CONCLUSION

In order to detect damage and evaluate the structural safety of the bridge piers impacted by low-speed vehicles, the frequency domain-based correlation technique (DCI), which was suggested in this work, was used. Its applicability and usefulness were confirmed. The study's findings led to the following deductions:

1. Measurements of the frequency response functions of the structures with impact damages were the primary methods in the suggested strategy, and the modal frequency parameters of the structures were obtained using the fast Fourier transform (FRFs) processing. The intrinsic frequencies of the columns were found to be significantly impacted by the cracking processes. Additionally, the impacts caused the modal frequencies to become nonmonotonic and the stiffness values of the columns at the crack sections to decrease. Therefore, the structural damage correlation indexes (DCI) can be calculated and compared using the collected data. The outcomes showed that residual stiffness values and the extent of structural damage may be accurately predicted by the DCI.
2. The finite element method-based computation methodologies for modal identification after structural damage and impact on reinforced concrete columns are presented, and the accuracy of the benchmark experimental model is confirmed.
3. The predamaged vehicle-pier impact events were calculated using a finite element method in the current study inquiry. The largest impact force was predicted using equation (20) and the DCI. It was demonstrated that the suggested formula had the benefit of accounting for the decreases in impact force and the loss of stiffness brought on by structural flaws when compared to the findings from related research projects. As a result, the suggested approach offered a useful foundation for subsequent stages of structural design.

REFERENCES

1. Cook W, Barr PJ and Halling MW. Bridge failure rate. J Perform Constr Facil 2015; 29: 04014080.
2. Gomes GF, Mende´z YAD, Alexandrino PSL, et al. The use of intelligent computational tools for damage detec- tion and identification with an emphasis on composites: a review. Compos Struct 2018; 196: 44–54.
3. Perez MA, Gil L and Oller S. Impact damage identifica- tion in composite laminates using vibration testing. Com- pos Struct 2014; 108: 267-276.
4. Zenzen R, Belaidi I, Khatir S, et al. A damage identifica- tion technique for beam-like and truss structures based on FRF and Bat algorithm. CR Me´canique 2018; 346: 1253–1266.
5. Liu S, Zhang L, Chen Z, et al. Mode-specific damage identification method for reinforced concrete beams: con- cept, theory and experiments. Constr Build Mater 2016; 124: 1090–1099.
6. Sha G, Cao M, Radzien´ski M, et al. Delamination- induced relative natural frequency change curve and its use for delamination localization in laminated composite beams. Compos Struct 2019; 230: 111501.
7. Sampaio RPC, Silva TAN, Maia NMM, et al. Damage identification based on response functions in time and frequency domains. In: Nobari AS and Ferri Aliabadi MH (eds) Vibration-based techniques for damage detection and localization in engineering structures. China: World Scientific Publishing Co Pte Ltd, 2018, pp. 197–236.
8. Pe´rez MA, Pernas-Sa´nchez J, Artero-Guerrero JA, et al. High-velocity ice impact

damage quantification in com- posite laminates using a frequency domain-based correla- tion approach. Mech Syst Signal Process 2021; 147: 107124.
9. Officials AAoSHaT. AASHTO-LRFD. Bridge design specifications – customary US Units. 5th ed. Washington, DC: Officials AaoSHaT, 2010.
10. Chen L, El-Tawil S and Xiao Y. Reduced models for simulating collisions between trucks and bridge piers. J Bridge Eng 2016; 21: 04016020.
11. Abdelkarim OI and ElGawady MA. Performance of bridge piers under vehicle collision. Eng Struct 2017; 140:337–352.
12. Al-Thairy H and Wang YC. An assessment of the current Eurocode 1 design methods for building structure steel columns under vehicle impact. J Constr Steel Res 2013; 88: 164–171.
13. Buth CE, Brackin MS, Williams WF, et al. Collision loads on bridge piers: phase 2, report of guidelines for designing bridge piers and abutments for vehicle collisions. Bryan, TX: Texas Transportation Institute, 2011.
14. Buth CE, Williams WF, Brackin MS, et al. Analysis of large truck collisions with bridge piers: phase 1, report of guidelines for designing bridge piers and abutments for vehicle collisions. Bryan, TX: Texas Transportation Insti- tute, 2010.
15. Chen L, Xiao Y, Xiao G, et al. Test and numerical simu- lation of truck collision with anti-ram bollards. Int J Impact Eng 2015; 75: 30–39.
16. Cai J, Ye JB, Chen QJ, et al. Dynamic behaviour of axially-loaded RC columns under horizontal impact loading. Eng Struct 2018; 168: 684–697.
17. Zhou XW, Zhou M, Gao YS, et al. An evaluation study on the cumulative impact damages of reinforced concrete piers based on modal frequencies. Eng Fail Anal 2021; 119: 104983.
18. Adhikary SD, Li B and Fujikake K. Dynamic behavior of reinforced concrete beams under varying rates of con- centrated loading. Int J Impact Eng 2012; 47: 24–38.
19. Pham TM and Hao H. Influence of global stiffness and equivalent model on prediction of impact response of RC beams. Int J Impact Eng 2018; 113: 88–97.
20. Chen L, Wu H and Liu T. Shear performance evaluation of reinforced concrete piers subjected to vehicle collision. J Struct Eng 2020; 146: 04020026.
21. Sharma H, Hurlebaus S and Gardoni P. Performance- based response evaluation of reinforced concrete columns subject to vehicle impact. Int J Impact Eng. 2012; 43: 52–62.
22. Murray YD. Users manual for LS-DYNA concrete material model 159. No. FHWA-HRT-05-062. Washing- ton, DC: United States Federal Highway Administration Office of Research, Development, and Technology, 2007.
23. Pastor M, Binda M and Harcˇarik T. Modal assurance cri- terion. Procedia Eng 2012; 48: 543–548.
24. Allemang RJ. The modal assurance criterion – twenty years of use and abuse. Sound Vib 2003; 37: 14–23.
25. Ahlgren P, Jarneving B and Rousseau R. Requirements for a cocitation similarity measure, with special reference to Pearson's correlation coefficient. J Am Soc Inform Sci Technol 2003; 54: 550–560.